Monte Carlo simulation of x-ray spectra generated by kilo-electron-volt electrons

X. Llovet[a)]
Serveis Cientificotècnics, Universitat de Barcelona, Lluís Solé i Sabarís 1-3, 08028 Barcelona, Spain

L. Sorbier
Institut Français du Pétrole, 1 et 4 avenue de Bois-préau, 92852 Rueil-Malmaison, France

C. S. Campos[b)], E. Acosta, and F. Salvat
Facultat de Física (ECM), Universitat de Barcelona, Diagonal 647, 08028 Barcelona, Spain

(Received 9 September 2002; accepted 13 December 2002)

We present a general algorithm for the simulation of x-ray spectra emitted from targets of arbitrary composition bombarded with kilovolt electron beams. Electron and photon transport is simulated by means of the general-purpose Monte Carlo code PENELOPE, using the standard, detailed simulation scheme. Bremsstrahlung emission is described by using a recently proposed algorithm, in which the energy of emitted photons is sampled from numerical cross-section tables, while the angular distribution of the photons is represented by an analytical expression with parameters determined by fitting benchmark shape functions obtained from partial-wave calculations. Ionization of K and L shells by electron impact is accounted for by means of ionization cross sections calculated from the distorted-wave Born approximation. The relaxation of the excited atoms following the ionization of an inner shell, which proceeds through emission of characteristic x rays and Auger electrons, is simulated until all vacancies have migrated to M and outer shells. For comparison, measurements of x-ray emission spectra generated by 20 keV electrons impinging normally on multiple bulk targets of pure elements, which span the periodic system, have been performed using an electron microprobe. Simulation results are shown to be in close agreement with these measurements. [DOI: 10.1063/1.1545154]

I. INTRODUCTION

An accurate description of x-ray spectra emitted from samples irradiated by kilo-electron-volt (keV) electron beams is of interest for quantitative electron probe microanalysis, especially for the analysis of samples with complex geometries (porous media, rough surfaces, submicron particles, etc.) or under grazing-exit conditions,[1], and in general for the characterization of medical and analytical x-ray sources.[2,3] Although, in principle, x-ray spectra can be computed from the numerical solution of the electron-transport equation,[4] Monte Carlo (MC) simulation has proven to be the most suitable method for the calculation of electron-induced x-ray spectra, mostly because it can incorporate realistic interaction cross sections and can be applied to targets with complex geometries.

The x-ray emission spectrum generated by keV electrons consists of characteristic peaks superimposed on a continuous background. The background is caused by bremsstrahlung photons and, to a lesser extent, by Compton-scattered characteristic x-rays. Characteristic peaks are produced by x rays emitted in radiative transitions of atoms that are ionized in an inner shell, either by electron impact or by photon absorption. The calculation of x-ray emission spectra by keV electrons is generally difficult, mostly because bremsstrahlung emission and inner-shell ionization occur with very small probabilities, in comparision with the dominant interaction mechanisms of elastic scattering and outer-shell ionization (or excitation). In practical MC simulations of keV electron transport, the description of x-ray emission mechanisms is frequently oversimplified and even disregarded, owing to their negligible stopping effect.

Simulations of x-ray spectra generated by keV electrons have been carried out by different authors (e.g., Refs. 5–7). In the majority of cases, only the electron transport is directly simulated and the photon generation and transport is described by other means. Moreover, comparison of simulation/calculation results with experimental spectra is usually made in relative terms, e.g., by normalizing the measured x-ray spectrum to the same area as the MC result, due to the fact that the conversion of measured spectra to absolute units requires knowledge of various instrumental parameters that are usually affected by large uncertainties.

Sempau *et al.*[8] described an algorithm for the simulation of coupled electron-photon transport, based on the use of the general-purpose simulation code PENELOPE.[9] As noted by the authors, owing to approximations in the cross sections of the various emission mechanisms, the algorithm was not appropriate for an accurate simulation of x-ray spectra generated by keV electrons. Acosta *et al.*[10] further developed the Sempau *et al.* algorithm and improved the generation of characteristic x rays by electron impact by using more elaborate

[a)]Author to whom correspondence should be addresed; electronic mail: xavier@giga.sct.ub.es
[b)]Permanent address: Instituto de Física, Universidade Federal do Rio Grande do Sul (UFRGS). 91501-970 Porto Alegre, RS. Brazil.

cross sections for K-shell ionization;[11] they also improved the intrinsic angular distribution of emitted bremsstrahlung photons at low energies by using an analytical approximate formula derived by Kirkpatrick and Wiedmann[12] (and subsequently modified by Statham).[5] Although the simulation results of Acosta *et al.*[10] were in fair agreement with measured absolute spectra, the adopted bremsstrahlung angular distribution was not yet accurate enough for quantitative purposes.[13] Moreover, the simulation code allowed only the simulation of K x rays, as the adopted electron-impact ionization cross sections were not appropriate for L and outer shells.

Recently, Acosta *et al.*[14] have proposed an algorithm for the simulation of bremsstrahlung emission in which (i) the energy of emitted photons is sampled from numerical energy-loss spectra obtained from the scaled cross-section tables of Seltzer and Berger[15] and (ii) the angular distribution is described by an analytical expression with parameters determined by fitting the benchmark partial-wave shape functions of Kissel, Quarles and Pratt.[16] Segui *et al.*,[17] on the other hand, have developed a computer code for calculating electron-impact ionization cross sections of neutral atoms using the distorted-wave Born approximation (DWBA). In the energy range of interest, DWBA calculations are formidably difficult, not only because of the very slow numerical convergence of the partial-wave series, but also because radial integrals must be calculated with high accuracy to prevent the accumulation of numerical errors. The calculation program of Segui *et al.*[17] overcomes these difficulties and reproduces experimental ionization cross section measurements of both K and L shells satisfactorily, as has been recently shown[18,19] for selected elements.

In the present article we describe an MC algorithm for the simulation of x-ray spectra emitted from targets bombarded by keV electrons, which incorporates the Acosta *et al.*[14] simulation of bremsstrahlung emission together with K- and L-shell ionization cross sections obtained from the DWBA calculations of Segui *et al.*.[17] The relaxation of ionized atoms is simulated by using transition probabilities from the Lawrence Livermore National Laboratory Evaluated Atomic Data Library (EADL).[20] As in our previous studies, the transport of electrons and photons is described by the standard, detailed method using the latest version of the general-purpose MC code PENELOPE.[21] To validate the simulation scheme, we have performed absolute measurements of x-ray emission spectra generated by 20 keV electron beams impinging normally on single-element targets using an electron microprobe. Measurements were performed on targets of 14 elements, which span the periodic system. Simulation results agree well with measured absolute spectra in the photon energy range between ~ 3 and ~ 15 keV, where the efficiency of the Si(Li) detector is approximately constant.

II. SIMULATION OF X-RAY EMISSION SPECTRA

A. Electron penetration and slowing down

Elastic scattering of electrons is simulated by using the modified Wentzel (MW) model. The MW differential cross section (DCS) is expressed as a combination of the Wentzel (screened Rutherford) DCS and a simple correcting distribution, which is either a fixed-angle distribution (a delta distribution) or a large-angle triangle distribution (for further details, see Ref. 21). The MW DCS model contains three parameters that are determined in such a way that the mean free path between collisions and the mean and the variance of the angular deflection in each elastic collision are identical with the values obtained from a realistic numerical DCS. The model is thus completely determined by the values of the mean free path and the first and second transport mean free paths, which have been calculated for all elements using a partial-wave method with the Dirac-Hartree-Fock field, corrected for exchange effects.[22]

Inelastic collisions are described in terms of the analytical DCS derived from the Lijlequist–Sternheimer generalized oscillator strength (GOS) model. In this model, the ionization of each atomic electron shell is described by a single δ oscillator, whose ''resonance energy'' is set in such a way that the mean ionization energy tabulated by Berger and Seltzer[23] is reproduced. The model yields stopping powers that coincide with the values recommended by Berger and Seltzer for energies above 10 keV, and is expected to remain accurate for much smaller energies, down to a few hundred electron volts. However, inner-shell ionization cross sections obtained from the Lijlequist–Sternheimer GOS model are only roughly approximate. Although their use in a Monte Carlo code is permissible, as inner-shell ionization is a low-probability process and has a very weak effect on the global electron-transport properties, the Lijlequist–Sternheimer GOS model is not appropriate for simulating inner-shell ionization and the subsequent emission of characteristic x rays. To overcome this difficulty we will consider inner-shell ionization as an independent interaction process, which has no effect on the projectile, and describe it using the more elaborate DWBA cross sections (see below).

B. Simulation of bremsstrahlung emission

The simulation of bremsstrahlung emission is performed by using the algorithm developed by Acosta *et al.*.[14] To be more specific, we consider the bremsstrahlung DCS for electrons of kinetic energy E in an amorphous, single-element medium of atomic number Z. After integrating over the angular deflection of the projectile, the DCS depends only on the energy W of the emitted photon and on the direction of emission, represented by the polar angle θ relative to the direction of the projectile, and can be expressed as

$$\frac{d^2\sigma}{dW\, d(\cos\theta)} = \frac{d\sigma}{dW} p(Z, E, \kappa; \cos\theta), \tag{1}$$

where $\kappa \equiv W/E$ is the reduced energy of the photon, $d\sigma/dW$ is the energy-loss DCS, differential only in the energy of the emitted photon and $p(Z, E, \kappa; \cos\theta)$ is the shape function, i.e., the probability distribution function (pdf) of $\cos\theta$ for given values of E and κ (normalized to unity).

The scaled bremsstrahlung DCS is defined as $(\beta^2/Z^2) W d\sigma/dW$, where $\beta = v/c$ is the velocity of the electron in units of speed of light. Seltzer and Berger[15,24] produced extensive tables of the scaled DCS for all the elements

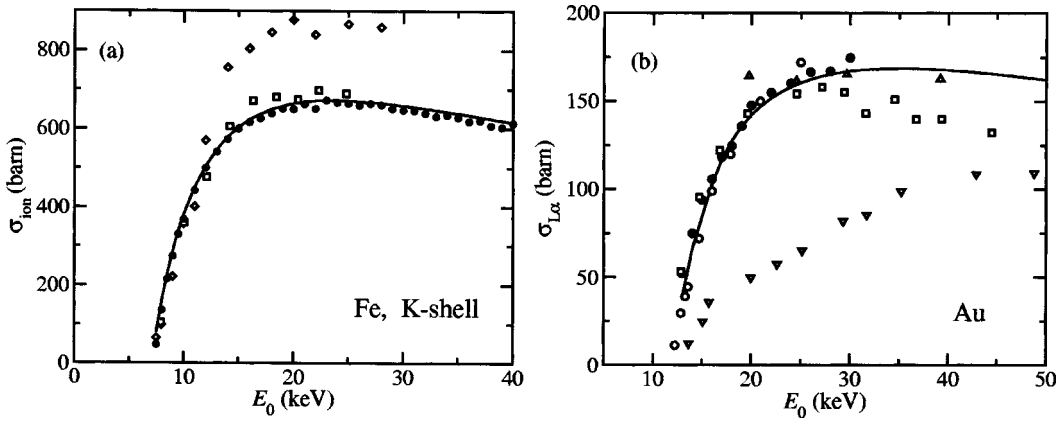

FIG. 1. Electron impact K-shell ionization cross section for Fe (a) and Lα x-ray production cross section for Au (b) vs incident electron energy. Solid lines are results from distorted-wave ionization cross sections calculated by Segui *et al.*[17] Symbols are experimental data from different sources.[19,30–33,25,35]

($Z=1-92$) and for electron energies from 1 keV to 10 GeV, which constitute the most reliable theoretical representation of bremsstrahlung energy spectra available at present. In the present study, the scaled DCS is obtained from Seltzer and Bergers's database,[15] and tabulated for a dense grid of electron kinetic energies, allowing accurate (and fast) linear interpolation in the variable ln$E$.

For the angular distribution of emitted photons $p(Z, E, \kappa; \cos\theta)$, we use the following expression:[14]

$$p(\cos\theta)=A\frac{3}{8}\left[1+\left(\frac{\cos\theta-\beta'}{1-\beta'\cos\theta}\right)^2\right]\frac{1-\beta'^2}{(1-\beta'\cos\theta)^2}+(1-A)\frac{3}{4}\left[1-\left(\frac{\cos\theta-\beta'}{1-\beta'\cos\theta}\right)^2\right]\times\frac{1-\beta'^2}{(1-\beta'\cos\theta)^2}, \tag{2}$$

with $\beta'=\beta(1+B)$. The parameters A and B are determined, by least-squares fitting, for the 144 combinations of atomic number, electron energy, and reduced photon energy corresponding to the benchmark partial-wave shape functions calculated by Kissel, Quarles, and Pratt.[16] The quantities ln($AZ\beta$) and $B\beta$ vary smoothly with Z, β, and κ and are obtained by cubic spline interpolation of their values for the benchmark cases. This permits the fast evaluation of the shape function for any combination of Z, β, and κ. Moreover, the random sampling of the photon direction, i.e., of $\cos\theta$, is performed by means of a simple and fast analytical algorithm.[14]

C. Inner-shell ionization

As already mentioned, the GOS model used to describe inelastic collisions is only appropriate for accounting for the average effect of such collisions on the primary electron. To obtain reliable inner-shell ionization distributions, more realistic cross sections for this process must be considered.

A consistent model for the simulation of x-ray emission must account for the following features of the process: (1) space distribution of inner-shell ionization along the projectile's track; (2) relative probabilities of ionizing various atomic electron shells, and (3) energies and emission probabilities of the electrons and x-rays released through the deexcitation cascade of the ionized atom. To determine the location of ionizing events and the atomic shell that is ionized we only need to consider total cross sections for ionization of individual inner shells. Here, we will adopt the DWBA cross sections computed by Segui *et al.*.[17]

To give a feel for the reliability of these DWBA ionization cross sections, in Fig. 1 we compare results from experimental measurements of K-shell ionization cross section for Fe and Lα x-ray production cross section ($\sigma_{L\alpha}$) for Au, with DWBA calculations. $L\alpha$ x-ray production cross sections were obtained by combining the corresponding ionization cross sections σ_{Li} for the different L subshells using the formula (see, e.g.,[25])

$$\sigma_{L\alpha}=\frac{\Gamma_{M4,5-L3}}{\Gamma_{\text{Total}-L_3}}\omega_{L_3}[\sigma_{L_3}+f_{23}\sigma_{L_2}+(f_{13}+f_{12}f_{23})\sigma_{L_1}], \tag{3}$$

where $\Gamma_{M_{4,5}-L_3}$ and $\Gamma_{\text{Total}-L_3}$ are the x-ray emission rates for the $L\alpha$ line ($M_{4,5}-L_3$ transition) and for all L lines ($M,N,O-L_3$ transitions), respectively, ω_{L_3} is the fluorescence yield for the L_3 shell and f_{ij} are the Coster–Kronig transition probabilities. These parameters were obtained by combining the corresponding transition probabilities extracted from the EADL.[20]

D. Atomic relaxation

In the present study, we simulate the emission of characteristic x-rays that result from vacancies produced in K shells and L subshells by photoelectric absorption, Compton scattering, and electron impact. These processes may leave the target atom in an ionized state with a vacancy in an inner shell (the probability of direct multiple ionization is negligibly small). We assume that the atomic relaxation process is independent of the mechanism by which the initial vacancy is created. In the simulation code, the relaxation of inner-shell vacancies is followed until the K and L shells are filled up, i.e., until the vacancies have migrated to M and outer

shells. Vacancies in these outer shells originate much less energetic secondary radiation (Auger electrons and x-rays), which only contributes in the low-energy portion of the x-ray spectrum.

The relaxation cascade is a sequence of (i) radiative transitions S0–S1 (an electron from the S1 shell fills the vacancy in the S0 shell, leaving a hole in the S1 shell) and (ii) nonradiative transitions S0–S1–S2 (an electron from the S1 shell fills the vacancy in the S0 shell, and the released energy is taken away by an electron in the S2 shell; this process leaves two vacancies, in the S1 and S2 shells). Nonradiative transitions of the type LI–LJ–Xq, which involve an electron transition between two L subshells and the ejection of an electron from an outer shell Xq are known as L shell Coster–Kronig transitions.

For each element in the medium, the information used to simulate the relaxation cascade consists of a table of possible transitions, transition probabilities, and energies of the released x-rays and electrons, for ionized atoms with a single vacancy in the K shell or in an L subshell. The energies of x-rays emitted in the radiative transitions are taken from Bearden.[34] For Auger emission, the energy of the emerging electron is obtained as the difference between the ionization energies of the shells involved. It is also assumed that the presence of additional vacancies, in the same or other shells, does not affect the emission energies. This assumption amounts to neglecting the relaxation of the emitting ion. Therefore, our approach will not produce L-shell satellite structures, which arise from the filling of a vacancy in a doubly ionized L shell (generated, e.g., by a Coster–Kronig transition), and release energy that is slightly different from the energy liberated when the shell contains only a single vacancy (because of the reduced screening of the nuclear charge due to the additional hole). As mentioned previously, multiple ionization is not considered and therefore our approach cannot produce the so-called hypersatellite lines, which arise when the ionization event leaves the atom with two holes in the same shell.

The transition probabilities are extracted from the EADL.[20] It is also worth recalling that such transition probabilities are approximate. For K shells they are expected to be accurate to within one percent or so, but for outer shells they are subject to much larger uncertainties.[26] Even the L-shell fluorescence yield (the sum of radiative transition probabilities for a vacancy in the L shell) is uncertain by about 20% (see, e.g., Refs. 20 and 39).

The simulation of the relaxation cascade is performed as follows. The transition that fills the initial vacancy is randomly selected according to the adopted transition probabilities, by using Walker's aliasing method.[27,28] This transition leaves the ion with one or two vacancies. If the energy of the emitted characteristic x-ray or Auger electron is larger than the corresponding absorption energy (i.e. the energy at which the tracking of particles is discontinued), the state variables of the particle are stored in the secondary stack (which contains the initial states of all particles produced during the current shower that have not yet been simulated). The generation of the cascade continues by repeating the process for each remaining vacancy. It ends either when the K shell and L subshells have been filled up or when there is not enough energy to produce ''active'' radiation, with energy larger than the absorption energy. The excitation energy of the residual ion is assumed to be deposited locally.

It is important to bear in mind that we are disregarding the emission and transport of soft x-rays and slow electrons. This sets a lower limit to the photon energies for which the present code is applicable. In principle, simulation results are expected to be reliable only for photons with energies larger than the ionization energy of the M1 subshell of the heaviest element present (125 eV for copper, 720 eV for silver, 3.4 keV for gold, and 5.5 keV for uranium).

E. Photon transport

The considered photon interactions are coherent (Rayleigh) scattering, incoherent (Compton) scattering, and photoelectric absorption. The cross sections implemented in PENELOPE are given by simple analytical formulas, with parameters determined from fits to updated interaction data from different sources. The DCS for coherent scattering is obtained from the Born approximation, with the atomic form factor given by a simple rational expression with parameters determined from a fit to the numerical form factors tabulated by Hubbell *et al.*[37] Compton scattering is simulated by means of the relativistic impulse approximation,[36] which accounts for Doppler broadening and binding effects. Photoelectric cross sections, are obtained by interpolation in a table generated with the XCOM program of Berger and Hubbell.[38,40] All random variables are generated by using purely analytical expressions, so that the structure of the simulation code is very simple.

F. Simulation algorithm

As already mentioned, our simulations are based on the general-purpose simulation code PENELOPE,[20] which is available from the Nuclear Energy Agency Data Bank.[29] The bremsstrahlung simulation algorithm and the description of the atomic relaxation cascade described above have been implemented into the latest version of PENELOPE.

Although PENELOPE can simulate electron tracks using a mixed procedure in which soft interactions are described by means of a multiple scattering approach, in the present study we operate the code in the detailed simulation mode, i.e., electron histories are generated interaction by interaction. The transport of photons is also described by the conventional detailed method. To improve the efficiency of the simulation, we apply interaction forcing[21] to both characteristic and bremsstrahlung emission processes. That is, we artificially shorten the mean free paths for these interactions and, accordingly, we redefine the weights of the generated secondary particles to keep the simulation results unbiased.

III. EXPERIMENTAL METHOD

X-ray spectra were acquired from thick samples of the elements Be, C, Si, Ti, Ni, Fe, Ge, Zr, Te, W, Pt, and Au on a CAMECA SX-50 electron microprobe, using a 20 keV electron beam at normal incidence. The spectra of emerging x-rays were analyzed with a Si(Li) energy-dispersive x-ray

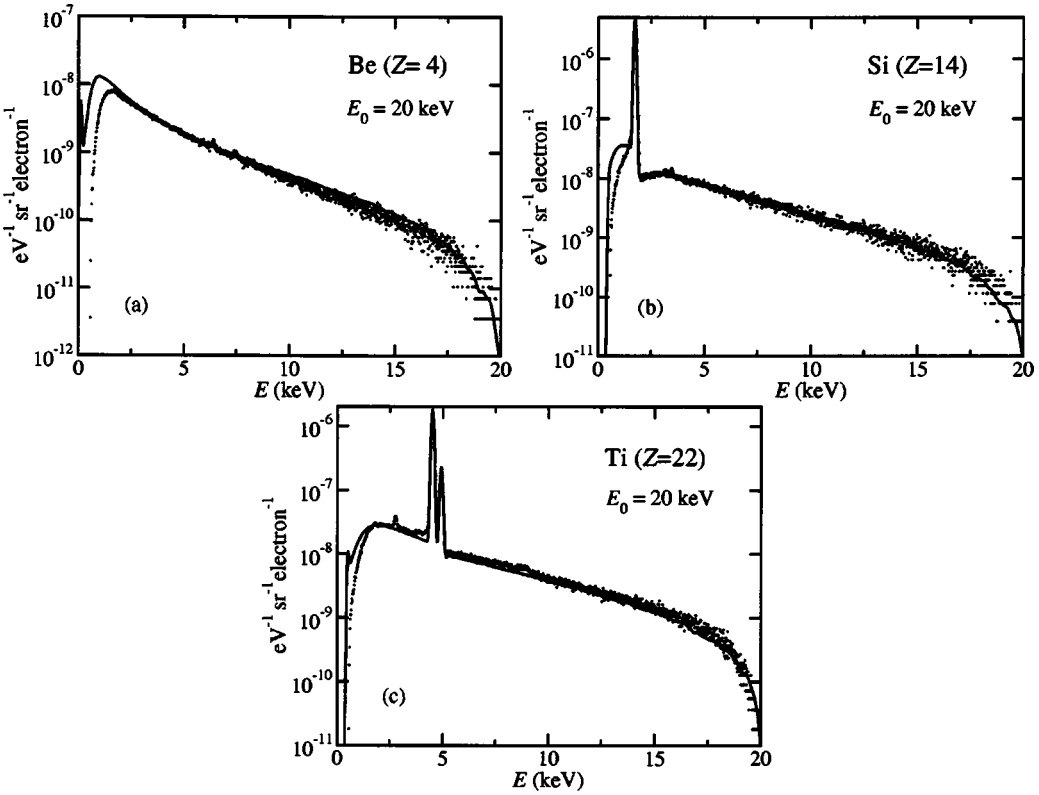

FIG. 2. Simulated (solid line) and experimental (dots) absolute x-ray spectra from berillium (a), silicon (b), and titanium (c) generated by 20 keV electron beams at normal incidence.

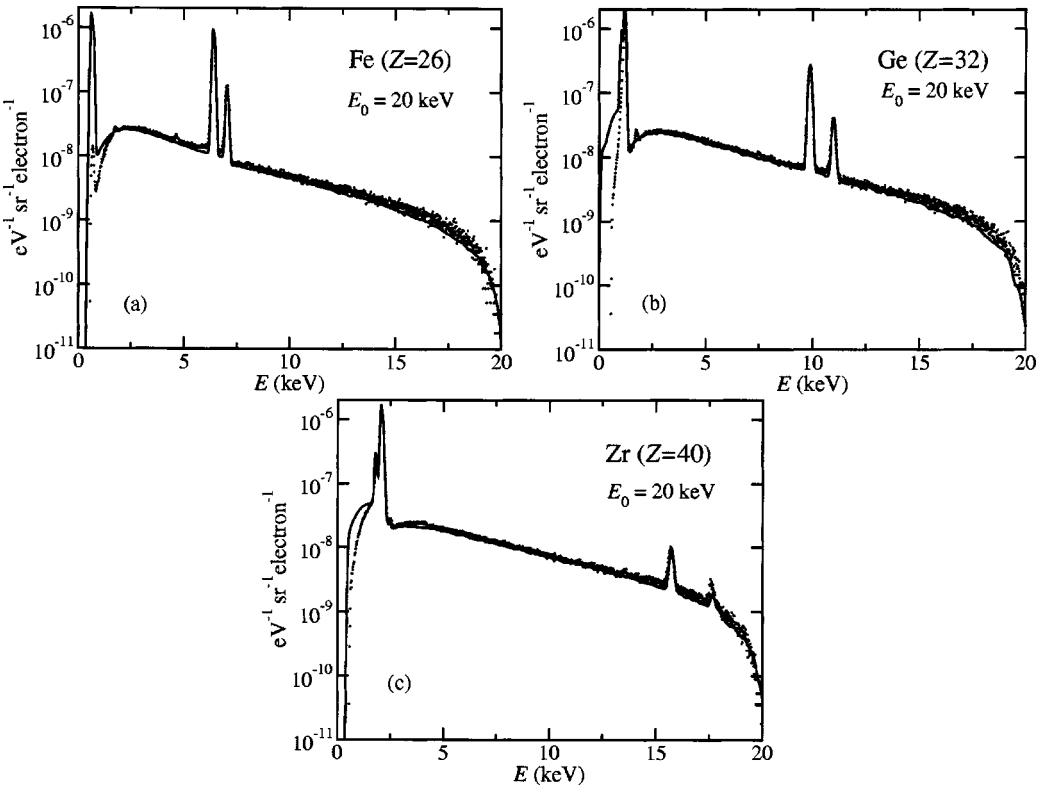

FIG. 3. Simulated (solid line) and experimental (dots) absolute x-ray spectra from iron (a), germanium (b), and zirconium (c) generated by 20 keV electron beams at normal incidence.

spectrometer, located in a direction forming an angle of 40° with the sample surface (take-off angle). Therefore, the x-ray emission angle is 130° with respect to the incident electron beam (i.e., reflection configuration). According to the manufacturer's specifications, the Si(Li) crystal is 3 mm thick and has an active area of approximately 12.5 mm^2. The detector has a 7-μm-thick beryllium window and a contact gold layer 0.02 μm thick. The thickness of the Si dead layer is 0.1 μm. The emerging photon beam is collimated with a diaphragm (300 μm in diameter) placed in front of the beryllium window, at 53 mm from the target. This minimizes spurious x-ray peaks caused by electrons backscattered onto the pole piece of the final lens of the microprobe column and other objects near the specimen. Probe currents were measured using a Faraday cup placed on the sample holder, and were chosen so as to yield a counting rate below 1000 counts per second, thus minimizing pulse pile-up effects. Typical acquisition times were about 1 h.

Acquired x-ray spectra were converted into absolute intensity units, i.e., number of photons emitted per unit energy interval and unit solid angle per incident (bombarding) electron, by using the equation

$$N(E)=\frac{N_{\mathrm{ch}}}{N_0\,\varepsilon(E)\,\Delta\Omega\,\Delta E}, \tag{4}$$

where N_{ch} is the number of counts in a particular photon energy channel, N_0 is the total number of incident electrons, $\Delta\Omega$ is the solid angle subtended by the x-ray detector, ΔE is the energy channel width, and $\varepsilon(E)$ is the detector efficiency; a function of the photon energy. The number of incident electrons N_0 was evaluated by multiplying the probe current I_0 by the acquisition time t. The width of the photon energy channel ΔE of the spectra is given by the energy-dispersive spectrometer software. The solid angle $\Delta\Omega$ was computed as A/d^2, where A is the area of the entrance aperture of the collimator, and d is the distance between the sample and the collimator. An estimation of the efficiency of the Si(Li) detector, using nominal values of the berillium window and crystal size, indicated that it is constant and close to unity in the photon energy range between 3 and 15 keV.[41,42] The limited information available on the internal structure of the Si(Li) detector did not allow us to estimate accurately the drop in efficiency outside this range. Hence, comparisons of simulated and measured spectra are meaningful only in the indicated interval of photon energies.

Uncertainties from counting statistics ranged typically from 3 to 8 % for the continuous component of the spectra, and were 1–2 % for most of the characteristic peaks. Using the values for A and d quoted by the manufacturer, the uncertainty in $\Delta\Omega$ was estimated to be less than 2%. The number of incident electrons was estimated to be accurate to within 2%. Other sources of systematic uncertainty, such as those associated with the take-off angle and target uniformity, are considered to be negligible. The various error contributions, added in quadrature, lead to an overall uncertainty of about 4–8 % for the continuous component of experimental spectra and less than 3% for the characteristic peaks.

IV. RESULTS AND DISCUSSION

To account for the response of the detector, simulated spectra were convoluted with a Gaussian distribution with an energy-dependent full width at half maximum (FWHM). The variation of the FWHM with the photon energy was estimated from measured x-ray spectra from different pure specimens, whose characteristic K x-ray energies span the region between 1–15 keV.

When comparing measured x-ray spectra with simulation results the following features should be considered. On the one hand, as mentioned previously, modeling of the physical processes in the simulation code is limited to energies larger than the ionization energy of the M1 subshell of the heaviest element present. As a consequence, M lines of the heaviest elements will not appear in the simulated spectra. On the other hand, we must recall that measured spectra are affected by various artifacts, such as incomplete charge collection, pulse pile-up, escape peaks, and sum peaks,[41,42] which cannot be totally avoided and whose effects are not included in the simulations.

In Figs. 2, 3, 4 we compare simulated and measured x-ray spectra generated by 20 keV electrons impinging at normal incidence on thick Be, Si, Ti, Fe, Ge, Zr, Te, W, and Pt targets. As indicated above, the comparison is meaningful only for the photon energy range from 3 to 15 keV, where the detector efficiency is nearly independent of the photon energy and close to unity. In general, agreement between simulation results and measurements is seen to be satisfactory. This agreement provides evidence for the reliability of the adopted interaction cross sections and for the accuracy of the simulation algorithm implemented in PENELOPE.

However, closer examination of the figures reveals that there are some systematic differences between simulation and experiment. In fact, if we rescale some of the experimental spectra, by dividing them by a constant so as to have the same area as the corresponding simulated spectrum in the range 3-15 keV, agreement between simulation and experiment improves. This is illustrated in Fig. 5, which compares simulated and experimental spectra in the above-mentioned photon energy range for C, Ni, and W. In the case of Ni and W, the experimental spectra were divided by factors 1.06 and 1.10, respectively, whereas for C, no rescaling was needed. By and large, the factors required to improve agreement between simulation and experiment seem to increase slightly with the target atomic number. Indeed, for the low-Z elements Be, C, and Si no systematic differences between simulation and experiment are observed, for medium-Z elements (Ti to Zr) differences are about 6-7 %, whereas for high-Z elements (Te to Au) experimental results are about $\sim$10% higher than simulation results.

The origin of these systematic and Z-dependent differences remains unclear. Presumably they could arise from inaccuracies in the adopted bremsstrahlung cross sections or from an instrumental artifact (a possible cause could be that electrons backscattered from the sample reach the detector). On the basis of the work of Kissel *et al.*,[16] the electron-nucleus component of the adopted scaled bremsstrahlung cross section is considered to be accurate to within 10%.

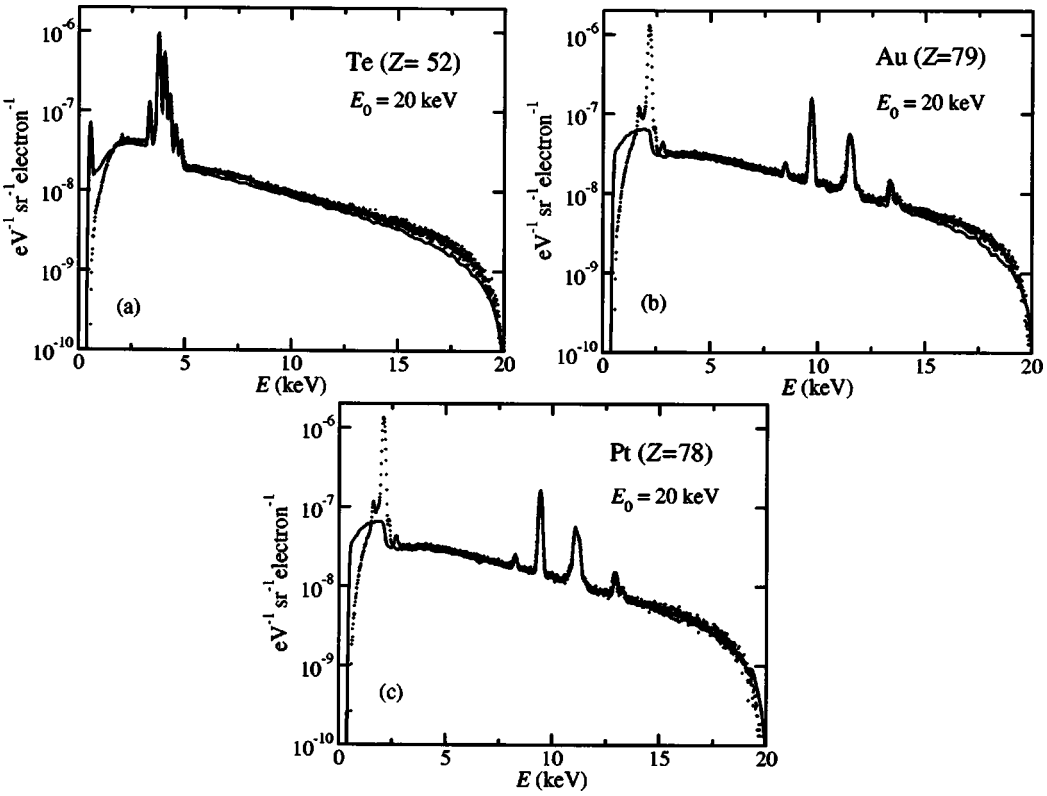

FIG. 4. Simulated (solid line) and experimental (dots) absolute x-ray spectra from tellurium (a), gold (b), and platinum (c) generated by 20 keV electron beams at normal incidence.

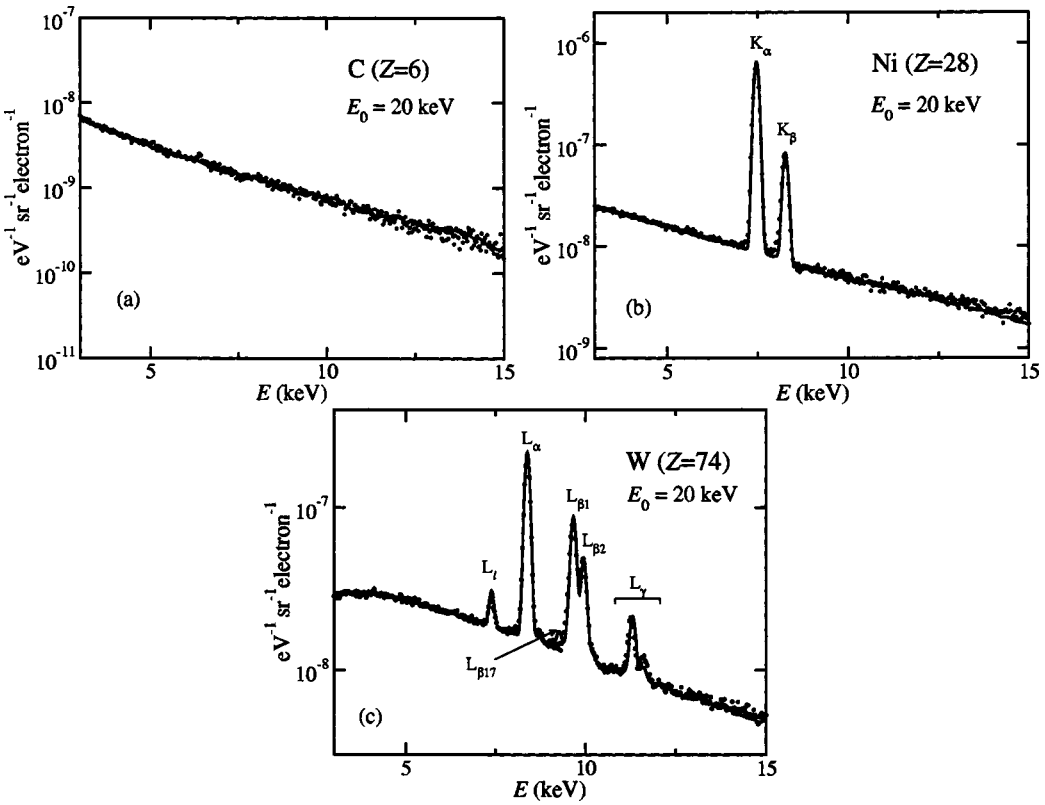

FIG. 5. Simulated (solid line) and experimental (dots) x-ray spectra from carbon (a), nickel (b), and tungsten (c) generated by 20 keV electron beams at normal incidence. In the case of nickel and tungsten, experimental spectra have been divided by a factor of 1.06 and 1.10, respectively.

There is also an uncertainty associated with the electron–electron contribution to the scaled bremsstrahlung cross section, whose relative importance increases when the atomic number decreases (roughly as Z^{-1}). It is also worth mentioning that the adopted shape functions (intrinsic angular distributions) pertain to the electron-nucleus bremsstrahlung, i.e., we have implicitly considered that the shape function for electron–electron bremsstrahlung is the same as for the nuclear component. Inaccuracies in the shape function would have an impact in the high-energy portion of the spectrum, near the bremsstrahling tip, as photons with energy close to that of the incident electron beam can only be emitted in the early stages of the penetration and slowing down process, when electrons still move essentially with their initial energy and in the direction of incidence. Under these circumstances, the detector ''sees'' the bremsstrahlung DCS with $\theta \simeq 130°$. Alternatively, let us assume that some of the electrons backscattered from the sample cross the Be window (and reach the sensitive volume of the detector) and/or generate bremsstrahlung within the Be window and the aperture. If so, whatever the origin, the ''spurious'' radiation will be detected as a smooth background in the x-ray spectrum, as pointed out by Statham.[5,42] As the number of backscattered electrons increases with atomic number, we cannot rule out the possibility that the observed differences, which also increase with the atomic number of the target, are partially due to ''spurious'' radiation caused by electron backscattering.

As seen in Figs. 2–5, some small discrepancies in the intensities of simulated and measured characteristic peaks are also observed. These differences are partially due to the uncertainties of the adopted ionization cross sections and relaxation parameters, as well as to the spectral artifacts mentioned above, namely, incomplete charge collection, pulse pile-up, and sum peaks. For the heavy elements W, Au, and Pt, the intensity of the $L\beta_{17}$ peak is overestimated in the simulated spectra, as is shown in Fig. 5(c) for W. For the same elements, a slight systematic shift of simulated $L\gamma$ peaks is also observed [see again Fig. 5(c)]. This shift originates from inaccuracies in the x-ray energies of the adopted database,[34] and could be amended by simply redefining the corresponding entries in the database.

ACKNOWLEDGMENTS

Financial support from the PICASSO Program No. HF2000-0053 (''Acciones Integradas entre España y Francia'') is gratefully acknowledged. C.S.C. wishes to acknowledge financial support from CNPq-Brasil (Project No. 200784/00-5).

[1] K. Tsuji, Z. Spolnik, and K. Wagatsuma, Spectrochim. Acta, Part B **56**, 2197 (2001).
[2] M. Bhat, J. Pattison, G. Bibbo, and M. Caon, Med. Phys. **26**, 303 (1999).
[3] S. Pepper and D. R. Wheeler, Rev. Sci. Instrum. **71**, 1509 (2000).
[4] D. B. Brown and J. V. Gilfrich, J. Appl. Phys. **42**, 4044 (1975).
[5] P.J. Statham, X-Ray Spectron **5**, 154 (1976).
[6] Z. J. Ding, R. Shimizu, and K. Obori, J. Appl. Phys. **76**, 7180 (1994).
[7] K. Araki, Y. Kimura, and R. Shimizu. Scanning Microsc. Suppl. **7**, 81 (1993).
[8] J. Sempau, E. Acosta, J. Baró, J. M. Fernández-Varea, and F. Salvat, Nucl. Instrum. Methods Phys. Res. B **132**, 377 (1997).
[9] J. Baró, J. Sempau, J. M. Fernández-Varea, and F. Salvat, Nucl. Instrum. Methods Phys. Res. B **100**, 31 (1995).
[10] E. Acosta, X. Llovet, E. Coleoni, J. A. Riveros, and F. Salvat, J. Appl. Phys. **83**, 6038 (1998).
[11] R. Mayol R and F. Salvat, J. Phys. B **23**, 2117 (1990).
[12] P. Kirkpatrick and L. Wiedmann, Phys. Rev. **67**, 321 (1945).
[13] N. S. Shin, Y. M. Koo, C. H. Chang, and H. Padmore, J. Appl. Phys. **86**, 902 (1999).
[14] E. Acosta, X. Llovet, and F. Salvat, Appl. Phys. Lett. **80**, 3228 (2002).
[15] S. M. Seltzer and M. J. Berger, At. Data Nucl. Data Tables **35**, 345 (1986).
[16] L. Kissel, C. A. Quarles, and R. H. Pratt, At. Data Nucl. Data Tables **28**, 381 (1983).
[17] S. Segui, E. Acosta, M. Dingfelder, J. M. Fernández-Varea, and F. Salvat (unpublished).
[18] X. Llovet, C. Merlet, and F. Salvat, J. Phys. B **35**, 973 (2002).
[19] C. Campos, M. A. Z. Vasconcellos, X. Llovet, and F. Salvat, Phys. Rev. A **66**, 012 719 (2002).
[20] S. T. Perkins, D. E. Cullen, M. H. Chen, J. H. Hubbell, J. Rathkopf, and J. Scofield, Report UCRL-50400 30 (Lawrence Livermore National Laboratory, Livermore, CA, 1991).
[21] F. Salvat, J. M. Fernández-Varea, E. Acosta, and J. Sempau, PENELOPE - *A code system for Monte Carlo simulation of Electron and Photon Transport*, (OECD/NEA Data Bank, Issy-les-Moulineaux, France, 2001). Available in PDF format from www.nea.fr.
[22] R. Mayol and F. Salvat, At. Data Nucl. Data Tables **65**, 55 (1997).
[23] M. J. Berger and S. M. Seltzer, *National Bureau of Standards, Report NBSIR 82-2550* Washington (1982); also available as ICRU Report 37 (1984).
[24] S. M. Seltzer and M. J. Berger, Nucl. Instrum. Methods Phys. Res. B **12**, 95 (1985).
[25] K. Shima, T. Nakagawa, K. Umetani, and T. Mikumo, Phys. Rev. A **24**, 72 (1981).
[26] C. J. Powell, in *Electron Impact Ionization*, edited by T. D. Mark and D. H. Dunn (Springer-Verlag, Berlin, 1985).
[27] A. J. Walker, ACM Trans. Math. Softw. **3**, 253 (1977).
[28] F. Salvat, Comput. Phys. Commun. **46**, 427 (1987).
[29] OECD Nuclear Energy Agency Data Bank. Le Seine Saint-Germain, 12 Boulevard des Iles, 92130 Issy-les-Moulineaux, France (e-mail: nea@nea.fr).
[30] F. Q. He, X.G. Long, X. F. Peng, Z. M. Luo, and Z. An, Acta Phys. Sin. **5**, 499 (1996).
[31] Z. M. Luo, Z. An, F. He, T. Li, L. M. Wang, and X. Y. Xia, J. Phys. B **230**, 2681 (1997).
[32] S. I. Salem and L. D. Moreland, Phys. Lett. **37A**, 161 (1971).
[33] D. V. Davis, V. D. Mistry, and C. A. Quarles, Phys. Lett. **38A**, 169 (1972).
[34] J. A. Bearden, Rev. Mod. Phys. **39**, 78 (1967).
[35] H. Schneider, I. Tobehn, F. Ebel, and R. Hippler, Phys. Rev. Lett. **71**, 2707 (1993).
[36] D. Brusa, G. Stutz, J. A. Riveros, J. M. Fernández-Varea, and F. Salvat, Nucl. Instrum. Methods Phys. Res. A **379**, 167 (1996).
[37] J. H. Hubbell, W. J. Veigele, E. A. Briggs, R. T. Brown, D. T. Cromer, and R. J. Howerton, J. Phys. Chem. Ref. Data **4**, 471 (1975); **6**, 615(E) (1977).
[38] M. J. Berger and J. H. Hubbell, National Bureau of Standards, Report NBSIR 87-3797, Washington (1987).
[39] J. H. Hubbell, P. N. Trehan, N. Singh, B. Chand, D. Mehta, M. L. Garg, R. R. Garg, S. Singh S, and S. Puri, J. Phys. Chem. Ref. Data **23**, 339 (1994).
[40] D. E. Cullen, M. H. Chen, J. H. Hubbell, S. T. Perkins, E. F. Plechaty, J. A. Rathkopf, and J. H. Scofield, Lawrence Livermore National Laboratory, Report UCRL-50400, Vol. 6, Rev. 4, Parts A and B (1989).
[41] H. D. Keith and T. C. Loomis, X-Ray Spectrom. **5**, 93 (1976).
[42] P. J. Statham, J. Microsc. **123**, 1 (1981).